



Synthesis, characterization, biological activity and equilibrium studies of metal(II) ion complexes with tridentate hydrazone ligand derived from hydralazine

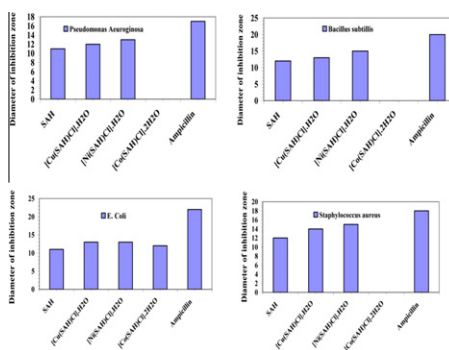
Ahmed A. El-Sherif, Mohamed M. Shoukry*, Mohamed M.A. Abd-Elgawad

Department of Chemistry, Faculty of Science, Cairo University, Cairo, Egypt

HIGHLIGHTS

- ▶ A new hydrazone ligand derived from the biologically active hydralazine was synthesised and characterized.
- ▶ Metal complexes were synthesised and characterized and showed promising biological activity.
- ▶ Stability and structural characterization of the complexes are supporting the biological activity of this class of complexes.
- ▶ Stability constant data is used to calculate the equilibrium distribution of the metal complexes in biological fluids.

GRAPHICAL ABSTRACT



ARTICLE INFO

Article history:

Received 18 June 2012

Received in revised form 10 August 2012

Accepted 14 August 2012

Available online 1 September 2012

Keywords:

Hydrazones
Metal(II)
Hydralazine
Electronic spectra
Stability constants
Biological activity

ABSTRACT

In the present study, a new hydrazone ligand (2-((2-phthalazin-1-yl)hydrazono)methyl)phenol) prepared by condensation of hydralazine (1-Hydralazinophthalazine) with salicylaldehyde (SAH). The synthesized SAH-hydrazone and its metal complexes have been characterized by elemental analyses, IR, ¹H NMR, solid reflectance, magnetic moment, molar conductance, mass spectra, UV–vis and thermal analysis (TGA). The analytical data of the complexes show the formation of 1:1 [M:L] ratio, where M represents Ni(II), Co(II) and Cu(II) ions, while L represents the deprotonated hydrazone ligand. IR spectra show that SAH is coordinated to the metal ions in a tridentate manner through phthalazine-N, azomethine-N and phenolic-oxygen groups. The ligand and their metal chelates have been screened for their antimicrobial activities using the disc diffusion method against the selected bacteria and fungi. Proton-ligand association constants of (SAH) and the stepwise stability constants of its metal complexes are determined potentiometrically in 0.1 M NaNO₃ at different temperatures and the corresponding thermodynamic parameters were derived and discussed. The order of $-\Delta G^\circ$ and $-\Delta H^\circ$ were found to obey $Mn^{2+} < Co^{2+} < Ni^{2+} < Cu^{2+}$, in accordance with the Irving–Williams order. The complexes were stabilized by enthalpy changes and the results suggest that the complexation is an enthalpy-driven process. The concentration distribution diagrams of the complexes are evaluated.

© 2012 Elsevier B.V. All rights reserved.

1. Introduction

Metal ions play essential roles in most of biochemical processes [1]. These ions can modify electron flow in a substrate, then

effectively controlling a specific reaction. Without the appropriate metal ion, a biochemical reaction would proceed very slowly, if at all. The interest in the study of hydralazine compounds has recently been grown up due to their biological activity and coordination capacity [2,3]. They find wide applications in the treatment of diseases such as tuberculosis, leprosy, and mental disorder. Also, they can be used as antihypertensive, antimicrobial, antimalarial

* Corresponding author. Tel.: +21 001834458; fax: +20 2 35728843.

E-mail address: shoukrymm@hotmail.com (M.M. Shoukry).

and antitumor [4]. The preparation of a new ligand was perhaps the most important step in the development of metal complexes which exhibit unique properties and novel reactivity. Since the electron donor and electron acceptor properties of the ligands, structural functional groups and the position of the ligand in the coordination sphere together with the reactivity of coordination compounds may be the factor for different studies [5,6]. Hydrazones were important class of ligands, such ligands have interesting ligation properties due to presence of several coordination sites [7]. Hydrazone ligands create an environment similar to biological systems by usually making coordination through oxygen and nitrogen atoms. Coordination chemistry of metal complexes of hydrazones [8] has gained a special attraction due to their biological activity and their ability to act as potential inhibitors for many enzymes [9]. Hydrazone derivatives possessing anti-inflammatory, analgesic [10], antipyretic [11], antibacterial [12] and antitumor [13] activities are also reported in the literature. With the above in mind, and in conjunction with our studies of metal complexes of biological significance [14–19], the present work is devoted to the preparation of hydrazone ligand derived from hydralazine with salicylaldehyde and its metal complexes. The study also includes biological activity of the synthesized complexes.

2. Experimental

2.1. Materials

All chemicals used in this investigation were laboratory pure including hydralazine, $\text{CuCl}_2 \cdot 2\text{H}_2\text{O}$, $\text{NiCl}_2 \cdot 6\text{H}_2\text{O}$, $\text{CoCl}_2 \cdot 6\text{H}_2\text{O}$, $\text{MnCl}_2 \cdot 4\text{H}_2\text{O}$, DMSO and salicylaldehyde were obtained from Sigma Chem. Co. Metal salt solutions were prepared and standardized as described previously [20]. NaOH solution (titrant) was prepared and standardized against potassium hydrogen phthalate solution. All solutions were prepared in deionized water.

2.2. Preparation of hydrazone ligand

The hydrazone ligand abbreviated as SAH was prepared by mixing an ethanolic solution (20 ml) of 2.01 g (0.01 mol) of salicylaldehyde with 1.13 g (0.01 mol) of hydralazine in the same volume

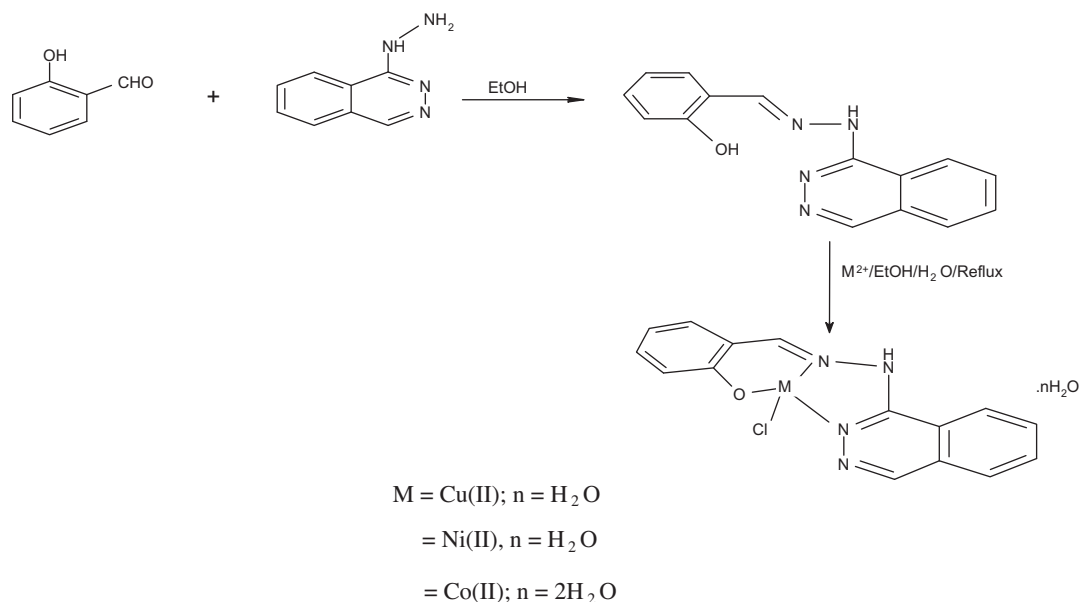
of ethanol and sodium acetate (3.46 g, 0.01 mmol) in 10 ml water as a buffering agent. The mixture then refluxed with stirring for 3 h. The product was left overnight then removed by vacuum filtration, washed several times by water, EtOH and Et_2O , and finally crystallized from EtOH. The ligand (HL) formed yellow crystals and yield 85%.

2.3. Preparation of the solid complexes

Copper(II), Nickel(II) and Cobalt(II) complexes of the SAH were prepared by direct mixing of 0.5 mmol of metal salt and the corresponding amount of SAH-hydrazone ligand and sodium acetate. The metal chloride was dissolved in water and ligand was dissolved in ethanol and sodium acetate in the smallest possible volume of water. The mixture was refluxed for 1–3 h. The formed solid complexes were separated by filtration and then washed several times with acetone and then diethyl ether. The solid complexes were dried in vacuum desiccator. The yield ranged from 79% to 82%. The complexes are soluble in ethanol, methanol, DMF and DMSO. The dried complexes were subjected to elemental and spectroscopic analysis.

2.4. Biological activity

Antimicrobial activity of the tested samples was determined using a modified Kirby-Bauer disc diffusion method [21]. Briefly, 100 μl of the test bacteria/fungi were grown in 10 ml of fresh media until they reached a count of approximately 108 cells/ml or 105 cells/ml for fungi [22]. 100 μl of microbial suspension was spread onto agar plates corresponding to the broth in which they were maintained. Isolated colonies of each organism that might be playing a pathogenic role should be selected from primary agar plates and tested for susceptibility by disc diffusion method of the National Committee for Clinical Laboratory Standards (NCCLS) [23]. Among the available media available, NCCLS recommends Mueller–Hinton agar due to: it results in good batch-to-batch reproducibility. Disc diffusion method for filamentous fungi tested by using approved standard method (M38-A) developed by the NCCLS [24] for evaluating the susceptibilities of filamentous fungi to antifungal agents. Disc diffusion method for yeasts developed by



Scheme 1. The general proposed structure for M^{II} -SAH complexes.

Table 1

Analytical and physical data of compounds.

Compound	M wt.	% Yield	Color	% Found (Calc.)				
				C	H	N	Cl	M
SAH	264.3	85%	Yellow	48.49 (48.17)	3.39 (4.58)	4.80 (21.20)	–	–
[Cu(SAH)Cl]·H ₂ O (1)	380.29	79%	Pale green	47.45 (47.37)	3.72 (3.45)	14.47 (14.73)	9.19 (9.32)	16.81 (16.71)
[Ni(SAH)Cl]·H ₂ O (2)	375.44	82%	Dark green	47.85 (47.99)	3.38 (3.49)	14.98 (14.92)	9.25 (9.44)	15.59 (15.63)
[Co(SAH)Cl]·2H ₂ O (3)	393.69	81%	Reddish brown	45.88 (45.76)	3.78 (3.84)	14.12 (14.23)	8.95 (9.01)	14.86 (14.97)

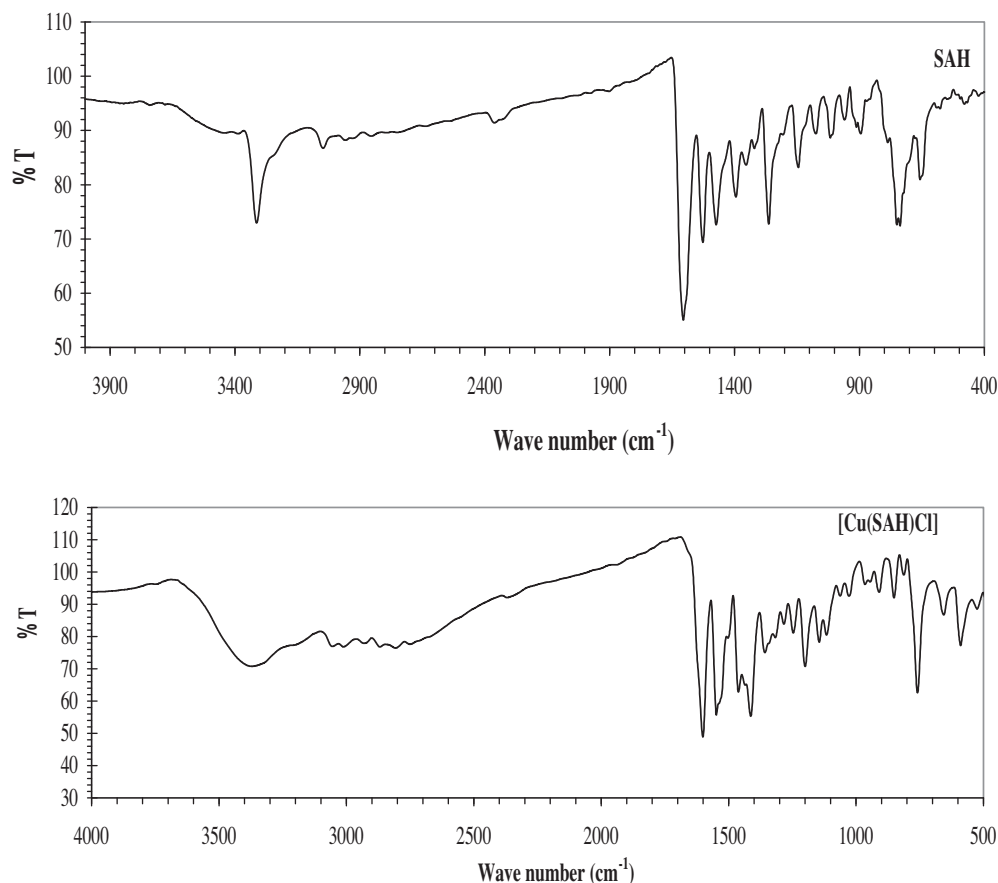
Table 2

Tentative assignment of the important infrared bands of the synthesized complexes.

Compound	$\nu(\text{cm}^{-1})$										
	$\nu(\text{H}_2\text{O})$	$\nu(\text{OH})$	$\nu(\text{C}=\text{N})$	$\delta(\text{O}-\text{H})$	$\nu(\text{C}-\text{O})_{\text{phenolic}}$	$\delta(\text{NH})$	$\nu(\text{NH})$	Ar-ring	$\nu(\text{M}-\text{N})$	$\nu(\text{M}-\text{O})$	$\nu(\text{M}-\text{Cl})$
SAH	–	3387	1607	1471	1263	1527	3315	960, 912, 786, 750	–	–	–
(1)	3365	–	1597	1462	1246	1548	3054	965, 909, 812, 758	520	467	345
(2)	3400	–	1602	1445	1249	1530	3016	943, 911, 841, 736	498	444	348
(3)	3410	–	1597	1454	1247	1535	3046	955, 918, 860, 747	594	457	352

using approved standard method (M44-P) by the NCCLS [25]. Plates inoculated with filamentous fungi as *Aspergillus flavus* at 25 °C for 48 h; Gram (+) bacteria as *Staphylococcus aureus*, *Bacillus subtilis*; Gram (–) bacteria as *Escherichia coli*, *Pseudomonas aeruginosa*, they were incubated at 35–37 °C for 24–48 h and fungi as *A. flavus* and *Candida albicans* incubated at 30 °C for 24–48 h and then the diameters of inhibition zones were measured in millimeters [21]. Standard discs of *Ampicillin* (Antibacterial agent), *Amphotericin B* (Antifungal agent) served as positive controls for antimicrobial activity but filter discs impregnated with 10 μl of

solvent were used as a negative control. The agar used is Mueller–Hinton agar that is rigorously tested for composition and pH. Further the depth of the agar in the plate is a factor to be considered in the disc diffusion method. This method is well documented and standard zones of inhibition have been determined for susceptible and resistant values. Blank paper disks (Schleicher and Schuell, Spain) with a diameter of 8.0 mm were impregnated with 10 μl of tested concentration of the stock solutions. When a filter paper disc impregnated with a tested chemical is placed on agar, the chemical will diffuse from the disc into the agar. This diffusion will

**Fig. 1.** FTIR of SAH-Schiff base ligand and [Cu(SAH)Cl] complex.

place the chemical in the agar only around the disc. The solubility of the chemical and its molecular size will determine the size of the area of chemical infiltration around the disc. If an organism is placed on the agar, it will not grow in the area around the disc if it is susceptible to the chemical. This area of no growth around the disc is known as a "Zone of inhibition" or "Clear Zone". For the disc diffusion, the zone diameters were measured with slipping calipers of the (NCCLS) [23]. Agar-based methods such as *E*-test and disk diffusion can be good alternatives because they are simpler and faster than the broth-based methods [26,27].

2.5. Instruments

The microchemical analysis of the separated solid chelates for C, H and N were performed in the microanalytical Center, Cairo University. The analyses were performed twice to check the accuracy of the analyses data. Infrared spectra were recorded on a 8001-PC FTIR Shimadzu spectrophotometer using KBr pellets. The solid reflectance spectra were measured on a Shimadzu 3101 pc spectrophotometer. The molar conductance of the complexes was measured for 1.00×10^{-3} M DMSO solutions at 25 ± 1 °C using a systronic conductivity bridge type 305. The room temperature magnetic susceptibility measurements for the complexes were determined by the Gouy balance using $\text{Hg}[\text{Co}(\text{SCN})_4]$ as a calibrant. A Shimadzu TGA-50H thermal analyzer was used to record simultaneously TG and DTG curves. The measurements were carried out in N_2 atmosphere (20 ml min^{-1}) with a heating rate of 10 °C min^{-1} in the temperature range 20–1200 °C using platinum crucibles, with a TGA-50 Shimadzu instrument.

Potentiometric measurements were made using a Metrohm 686 titroprocessor equipped with a 665 Dosimat (Switzerland-Herisau). A thermostated glass-cell was used equipped with a magnetic stirring system, a Metrohm glass electrode, a thermometric probe, a microburette delivery tube and a salt bridge connected with the reference cell filled with 0.1 M KCl solution in which saturated calomel electrode was dipped. Temperature was maintained constant inside the cell at 25.0 ± 0.02 °C, by the circulating water by a thermostated bath (precision ± 0.02). All potentiometric measurements in this study were carried out in Dimethylsulphoxide (DMSO)-water mixture containing 70% DMSO because of low solubility of hydrazone ligand and possible hydrolysis in aqueous solution.

2.6. Potentiometric titrations

The potentiometric cell was calibrated before each experiment to convert the pH meter readings into hydrogen ion concentration as reported in literature [28]. The ionic product ($K_w = [\text{H}^+][\text{OH}^-]$) were calculated at a constant ionic strength of 0.10 mol-dm^{-3} with NaNO_3 in 70% aqueous DMSO solutions based on measurements of $[\text{OH}^-]$ and pH in several series of experiments. We calculated the reproducible values of $\text{p}K_w$ for the examined 70% aqueous dimethyl sulfoxide solution [29]. The $\text{p}K_w$ value obtained is 15.75 in this medium. The following mixtures were prepared and titrated potentiometrically with 0.05 M NaOH solution.

- 50 ml of solution containing 8.0×10^{-4} M Metal(II) ion of constant ionic strength 0.1 M NaNO_3 .
- 50 ml of solution containing 8.0×10^{-4} M SAH ligand + 1.6×10^{-3} M HNO_3 of constant ionic strength 0.1 M (adjusted with NaNO_3);
- 50 ml of solution containing 8.0×10^{-4} M Metal(II) ion, 1.6×10^{-3} M SAH ligand + 1.6×10^{-3} M HNO_3 of constant ionic strength 0.1 M NaNO_3 .

The hydrolysis constants of metal(II) were determined by titrating mixture (a). The protonation constants of SAH were

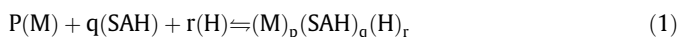
Table 3

Molar conductance, magnetic moment and electronic spectral data of Cu-SAH complexes.

Complex	Λ_M^a	μ_{eff} (BM)	λ_{max} (cm^{-1})
SAH	–	–	25,974, 34,722
$[\text{Cu}(\text{SAH})\text{Cl}]\cdot\text{H}_2\text{O}$ (1)	12.9	1.85	27,100, 17,094
$[\text{Ni}(\text{SAH})\text{Cl}]\cdot\text{H}_2\text{O}$ (2)	10.5	0	22,222, 15,552
$[\text{Co}(\text{SAH})\text{Cl}]\cdot 2\text{H}_2\text{O}$ (3)	11.2	2.55	19,417

^a Molar conductance measured for 10^{-3} M DMSO solution, $\Omega^{-1} \text{ cm}^2 \text{ mol}^{-1}$.

determined potentiometrically by titrating mixture (b). The formation constants of M(II)-SAH were determined by titrating mixture (c). All titrations were performed in a purified N_2 atmosphere, using aqueous 0.05 M NaOH as titrant.



$$\beta_{\text{pqr}} = \frac{[(\text{M})_p(\text{SAH})_q(\text{H})_r]}{[\text{M}]^p[\text{SAH}]^q[\text{H}]^r} \quad (2)$$

Caution!

Although no problems were encountered in this work, but it should be pointed out that for DMSO solutions only glass equipment and Hamilton Teflon valves can be used!

2.7. Data processing

The calculations were obtained from ca. 100 data points in each titration using the computer program MINQUAD-75 [30]. The

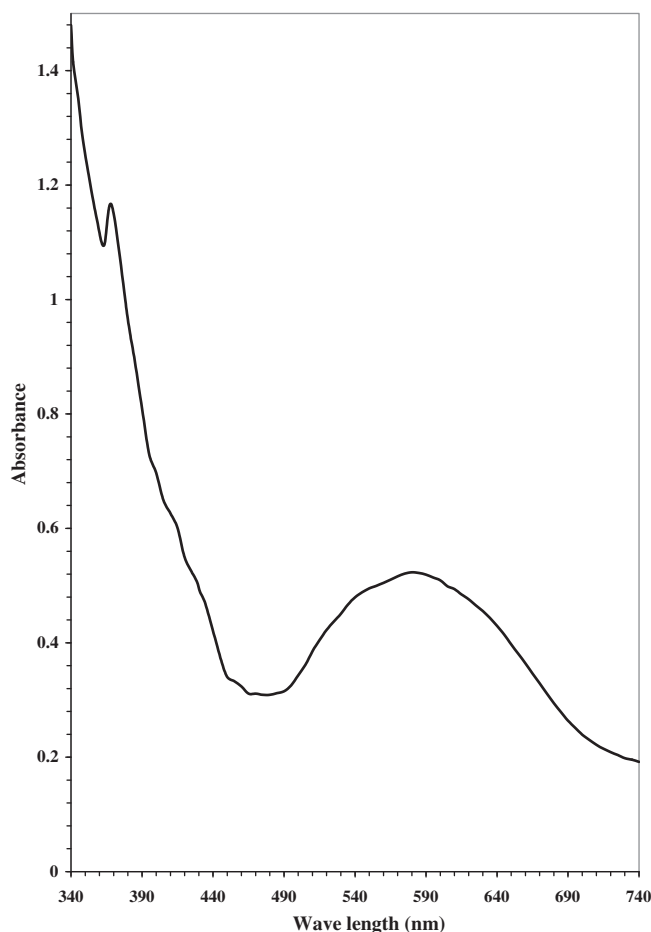


Fig. 2. Electronic spectra of Cu-SAH complex.

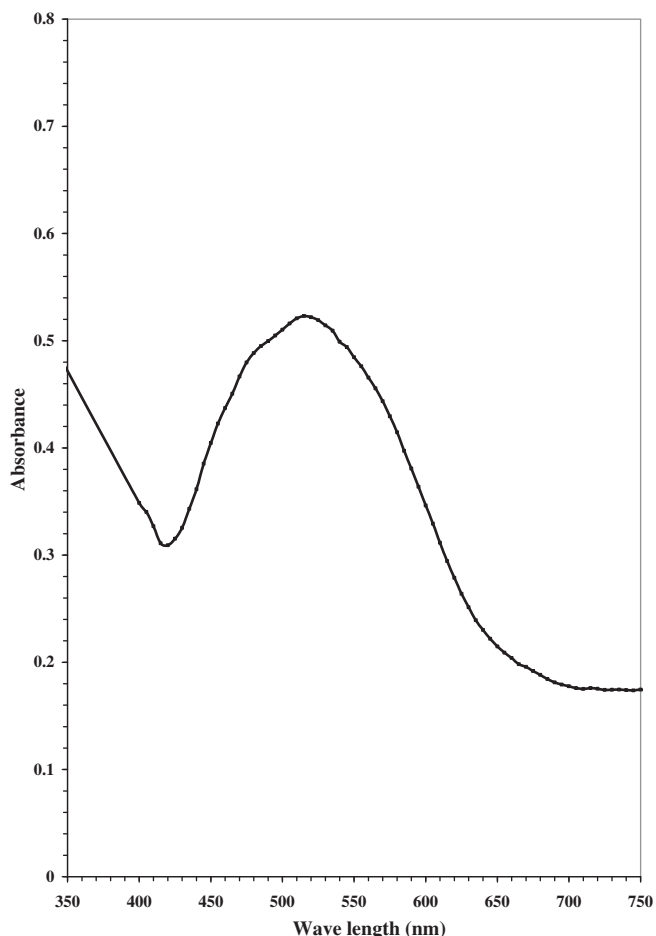


Fig. 3. Electronic spectra of Co-SAH complex.

stoichiometry and stability constants of the complexes formed were determined by trying various possible composition models. The model selected gave the best statistical fit and was chemically consistent with the titration data without giving any systematic drifts in the magnitudes of various residuals, as described elsewhere [30]. The fitted model was tested by comparing the experimental titration data points and the theoretical curve calculated from the values of the acid dissociation constant of the ligand and the formation constants of the corresponding complexes. The species distribution diagrams were obtained using the program SPECIES [31] under the experimental condition employed. All measurements were carried out in our laboratory in Cairo University.

3. Results and discussion

The condensation of salicylaldehyde with hydrazine in boiling ethanol yields a hydrazone compound (SAH). The chemical equations concerning the formation of the hydrazone and the complexes represented in Scheme 1. The interaction of SAH ligand and metal(II) salts in EtOH under reflux conditions gave the products presented in Table 1.

3.1. Elemental analysis

The elemental analysis data of the SAH ligand and its complexes are given in Table 1. The data show the formation of $[M(\text{SAH})\text{Cl}]$ in the complexes (where SAH represents the deprotonated hydrazone ligand). We found that the theoretical values are in a good agreement with the found values.

3.2. Molar conductance measurements

By using the relation: $\Lambda_M = K/C$, the molar conductance values of the prepared complexes with the mentioned metal ions under investigation were determined using 1×10^{-3} M DMSO solution, are in the range of $10.5\text{--}12.9 \Omega^{-1} \text{cm}^2 \text{mol}^{-1}$. These values indicated that, all synthesized complexes are nonelectrolytes. This is in accordance with the fact that conductivity values for a nonelectrolyte are below $50 \Omega^{-1} \text{cm}^2 \text{mol}^{-1}$ in DMSO solution [32,33]. Conductivity measurements are in a good agreement with the elemental analysis data, where Cl^{-1} ions are detected by addition of AgNO_3 solution, inside the coordination sphere of the complexes by the dissolving of the all complexes using nitric acid.

3.3. IR spectra and mode of bonding

The IR spectra in the ($4000\text{--}400 \text{cm}^{-1}$) region provide information regarding the coordination mode in the complexes were analyzed by comparison with the data for the free ligand. The most relevant bands and proposed assignments for all complexes along with the hydrazone ligand (SAH) ligand are given in Table 2. The IR-spectra of free hydrazone ligand and its Cu(II)-complex are shown in Fig. 1.

The IR spectrum of the free hydrazone ligand (SAH) reveals bands at 3387cm^{-1} may be assigned to $\nu(\text{OH})$ and $\nu(\text{NH})$ respectively. The $\nu(\text{OH})$ band is absent in the spectra of metal complexes, indicating coordination through the deprotonated phenolic OH group [34, 35]. Also, the participation of the OH group in coordination is apparent from the shift in position of the $\delta(\text{OH})$ in-plane bending at 1471cm^{-1} [36] in the free ligand by $11\text{--}24 \text{cm}^{-1}$ in the complexes and formation of M–O bond via deprotonation. Moreover, it was evidenced from the shift in the position of $\nu(\text{C–O})$ at 1263cm^{-1} [37] to the lower frequency region in the spectra of complexes

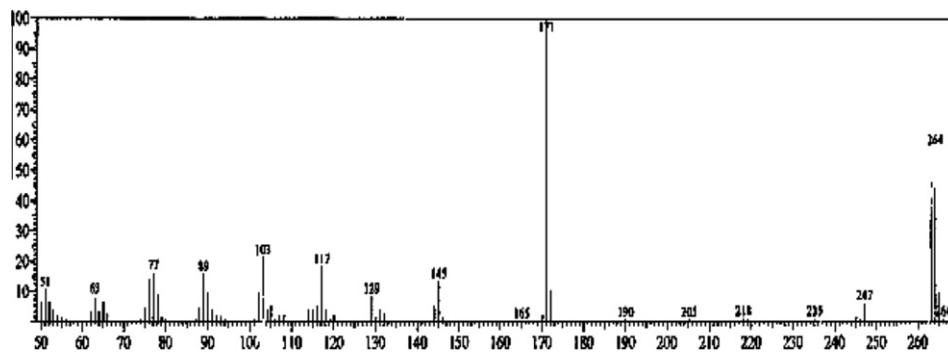


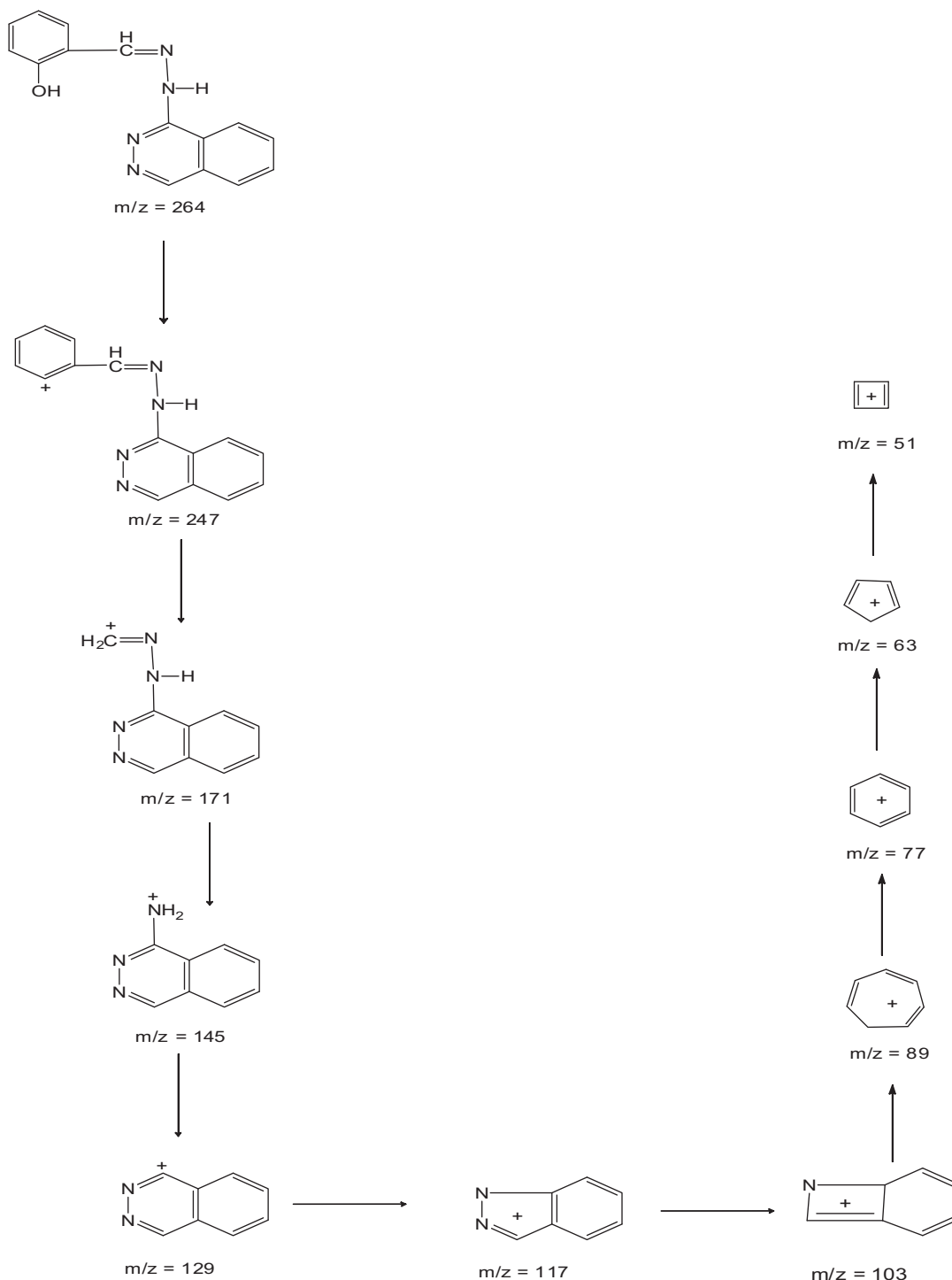
Fig. 4. Mass Spectrum of SAH-Schiff base.

[38]. However, the strong band observed at 1607 cm^{-1} in the free SAH ligand due to azomethine group vibration is shifted towards lower frequencies in the complexes, suggesting that azomethine group is involved in coordination [39–42]. Bands appearing at 960, 912, 786, 750 cm^{-1} are the usual modes of aromatic ring vibrations. The previously bands corresponding to aromatic moiety reveal small shifts in the resulted complexes than free ligand, this is usual due to the expected electronic structure changes upon complexation. The appearance of new bands in the low frequency ranges at 498–594 and $444\text{--}476\text{ cm}^{-1}$ due to $\nu(\text{M-O})$ and $\nu(\text{M-N})$

vibrations [43] respectively, support the participation of the nitrogen atom of the azomethine group and oxygen of the OH group of the ligand in the complexation with metal ions [43] as shown in Scheme 1.

All the complexes exhibit a band at $345\text{--}352\text{ cm}^{-1}$ originating from a $\nu(\text{M-Cl})$ vibration indicating the presence of chloride coordination thus completing the square-planar geometry for the present series of complexes [44].

As a general conclusion, the hydrazone ligand (SAH) participated in bonding to metal(II) as monobasic tridentate (N,N,O



Scheme 2. Mass fragmentation pattern of SAH hydrazone ligand.

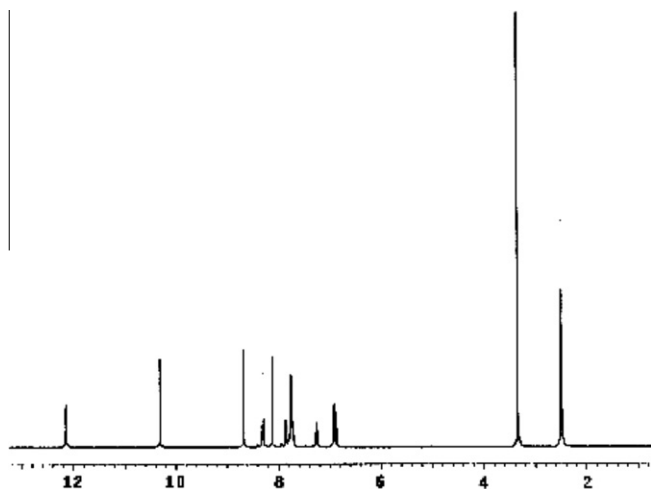


Fig. 5. ^1H NMR of SAH-Schiff base.

donor) ligand (Scheme 1). The nonelectrolytic nature of the complexes was evidenced from the low values of the molar conductance of the complexes measured in DMSO (Table 3).

3.4. Electronic spectra and magnetic properties

As the result of failure to obtain a single crystal for X-ray analyses to confirm the geometric structure for these complexes, solid

reflectance spectra and magnetic moment measurements are used for this purpose. The solid reflectance spectra of metal complexes show different bands at different wavelengths, each one is corresponding to certain transition which suggests the geometry of the complex compounds. In general, the d–d bands of copper(II) complexes for which a square planar structure has been proposed to occur in the range $16,000\text{--}20,000\text{ cm}^{-1}$ [45]. The electronic spectra of the $[\text{Cu}(\text{SAH})\text{Cl}]$ complex (Fig. 2) showed d–d absorption band centered at $17,094\text{ cm}^{-1}$ due to $^2\text{B}_{1g} \rightarrow ^2\text{A}_{1g}$ as reported for square planar Cu(II) complex [46,47]. As is known, magnetic susceptibility measurements provide information to characterize the structure of the complexes. The magnetic moments of the complexes were measured at room temperature and are listed in Table 3. The room temperature magnetic moment for $[\text{Cu}(\text{SAH})\text{Cl}]$ complex ($\mu_{\text{eff}} = 1.85\text{ BM}$) falls in the normal range for copper(II) species with $S = 1/2$ and this confirms that the copper(II) complex has square-planar geometry [48] with $d_{x^2-y^2}$ ground state [49].

The electronic spectrum of the diamagnetic nickel(II) complex (2) (Table 3) showed two absorption bands at $15,552$ and $22,222\text{ cm}^{-1}$ which may be assigned to the $^1\text{A}_{1g} \rightarrow ^1\text{B}_{2g}$, $^1\text{A}_{1g} \rightarrow ^1\text{B}_{1g}$ transitions, respectively, around Ni(II) in a square-planar geometry [50]. The assumed square planar geometry for this complex is confirmed from the value of its room temperature magnetic moment of zero [51].

The room temperature magnetic moment of $[\text{CoSAH})\text{Cl}]$ of 2.55 BM is more than that of low spin octahedral and lower than the values characteristic of tetrahedral cobalt(II) complexes. Furthermore, these values are similar to that reported for the square planar cobalt(II) complexes [52–54]. The electronic spectrum of

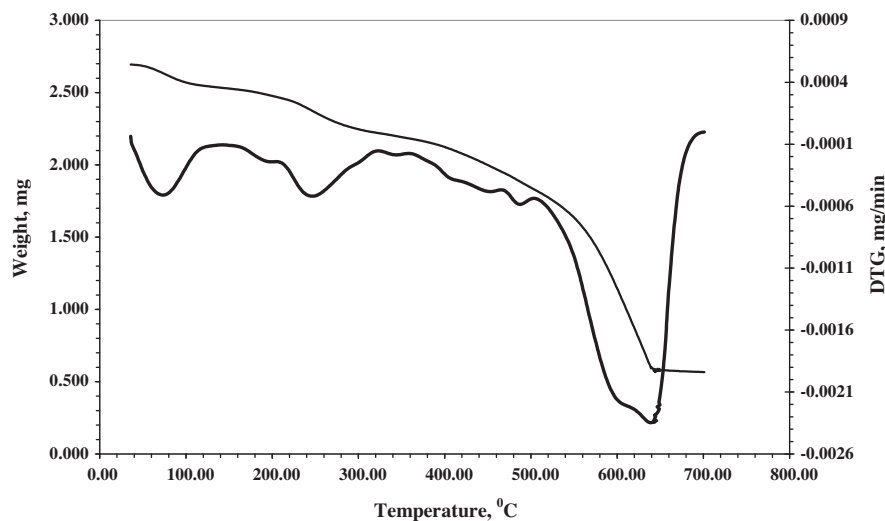


Fig. 6. TG and DTG of $[\text{Cu}(\text{SAH})\text{Cl}] \cdot \text{H}_2\text{O}$ complex.

Table 4
Stepwise thermal degradation data obtained from TGA curves for $\text{M}^{\text{II}}\text{-SAH}$ complexes.

Complex	Molar mass	TG range ($^{\circ}\text{C}$)	DTG _{max} (K)	Weight loss		Predicated intermediates and final products	Metallic residue found (calcd.%)
				Found	Calcd.		
(1)	380.29	48–104	73	4.58	4.73	H_2O	CuO 20.84 (20.91)
		104–270	246	9.56	9.33	$1/2\text{Cl}_2$	
		474–510	487	18.35	18.93	$2\text{N}_2 + \text{CH}_4$	
		510–675	639	46.4	46.1	C_{14}H_6	
(2)	374.54	43–180	90	4.31	4.80	H_2O	NiO 20.26 (20.03)
		259–532	436	28.85	28.75	$2\text{N}_2 + 1/2\text{Cl}_2 + \text{CH}_4$	
		532–776	673	46.58	46.45	C_{14}H_6	
(3)	393.69	41–120	76	9.43	9.14	$2\text{H}_2\text{O}$	CoO 18.14 (19.12)
		228–367	355	9.17	9.01	$1/2\text{Cl}_2$	
		367–402	379	7.21	7.11	N_2	
		402–659	459	56.05	55.62	Phthalazine + C_7H_5	

Table 5
The kinetic parameters for the non-isothermal decomposition of the complexes.

Range (°C)	T^a	E_a (kJ mol ⁻¹)	ΔH^* (kJ mol ⁻¹)	ΔS^* (JK ⁻¹ mol ⁻¹)	ΔG^* (kJ mol ⁻¹)
<i>[Cu(SAH)Cl]·H₂O</i> (1)					
48–104	73	42.36 ± 2.54	-38.05 ± 3.80	-205.35 ± 35.22	33.00 ± 18.30
104–270	246	12.82 ± 0.76	-6.50 ± 3.20	-328.41 ± 46.41	163.94 ± 73.07
474–510	487	7.81 ± 0.46	-0.233 ± 0.02	-347.20 ± 52.78	263.64 ± 103.64
510–675	639	37.60 ± 2.25	-37.60 ± 6.89	-319.15 ± 44.29	253.46 ± 101.8
<i>[Ni(SAH)Cl]·H₂O</i> (2)					
43–180	90	17.30 ± 1.04	-11.41 ± 1.84	-298.52 ± 41.20	96.95 ± 62.23
259–532	436	66.09 ± 3.96	-58.23 ± 7.98	-259.96 ± 37.31	126.09 ± 71.35
533–776	673	21.10 ± 1.27	-21.10 ± 2.94	-347.10 ± 55.23	307.25 ± 109.21
<i>[Co(SAH)Cl]·2H₂O</i> (3)					
41–120	76	28.37 ± 1.70	-23.16 ± 3.11	-253.88 ± 63.32	65.45 ± 24.22
228–367	355	16.20 ± 0.97	-10.79 ± 4.32	-330.94 ± 50.21	197.05 ± 89.11
367–402	379	16.12 ± 0.96	-10.04 ± 4.11	-308.16 ± 44.98	190.88 ± 88.78
404–659	459	44.51 ± 2.67	-44.52 ± 8.02	-299.35 ± 42.02	174.61 ± 81.45

^a The peak temperature from the DTG curve (°C).

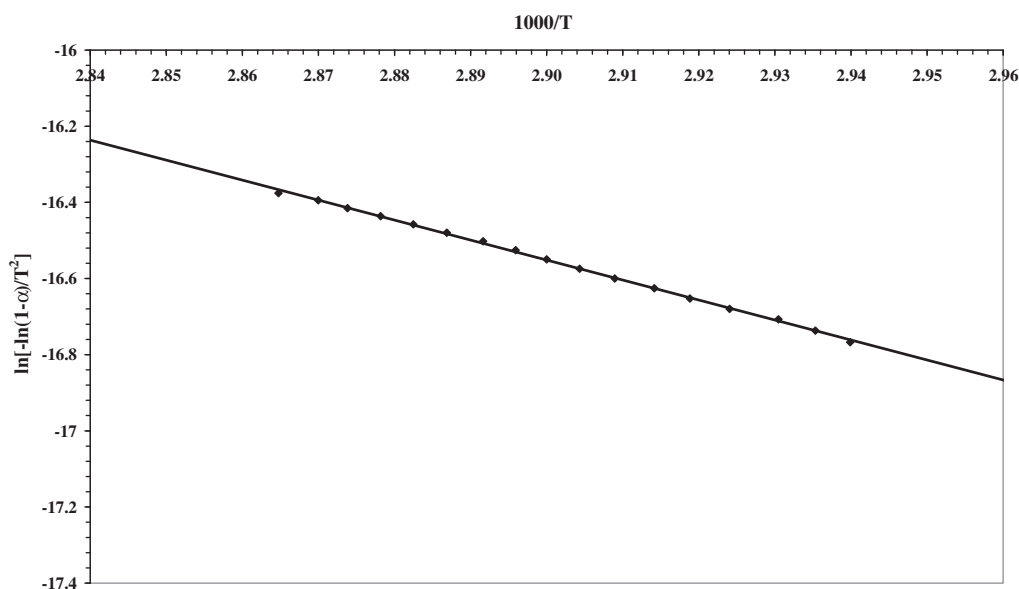


Fig. 7. Coats-Redfern linear plot for *[Cu(SAH)Cl]·H₂O* complex.

the complex, Fig. 3, exhibits a band at 19,417 cm⁻¹ characteristic of square planar cobalt(II) complexes [55].

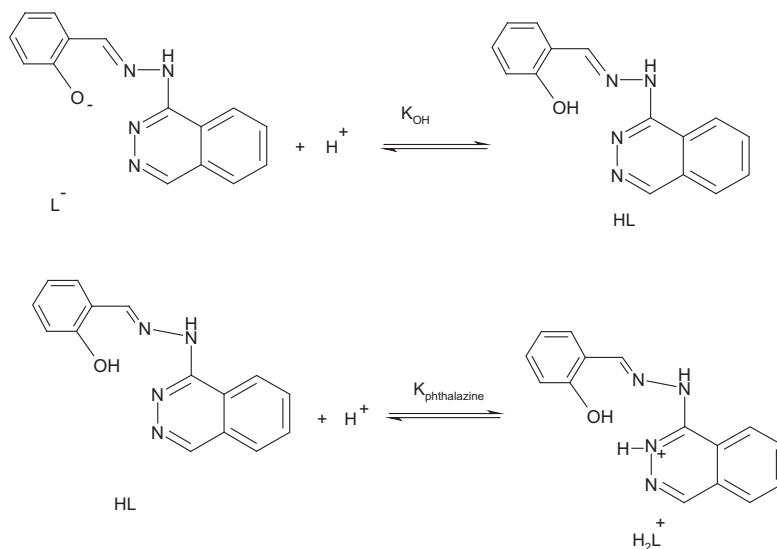
3.5. Mass spectra

The electron impact mass spectra of SAH- hydrazone ligand are recorded and investigated at 70 eV of electron energy. The mass spectra of the studied hydrazone ligand are characterized by moderate to high relative intensity molecular ion peaks. The mass spectrum of SAH, and the possible molecular ion peaks with their respective relative intensities are shown in Fig. 4. The mass spectra of SAH and the molecular ion peaks of the different suggested fragments are shown in Scheme 2. Their signals give an idea about the construction of ligand. Scheme 2 demonstrates the proposed path of the decomposition steps for the investigated hydrazone ligand. SAH shows a parent peak at $m/z = 264$ with a relative intensity = 54% (C₁₅H₁₂N₄O, calculated atomic mass 264 amu) represents the molecular ion peak of the SAH hydrazone ligand. The other molecular ion peaks (171 (100%), 145 (13.5%), 129 (9%), 117 (18%), 103 (21%), 89 (16%), 77(17%), 63 (9%) and 51 (11%)) appeared in the mass spectra are attributed to the fragmentation of SAH molecule obtained from

Table 6
Association constants of (SAH) at different temperatures at (70% DMSO-30% H₂O).

System	Temp. (°C)	log β ^a	S ^b
<i>SAH</i>			
(1) L ⁻ + H ⁺ ⇌ HL	20	11.11 ± 0.05	1.1E - 7
(2) L ⁻ + 2H ⁺ ⇌ H ₂ L ⁺		15.46 ± 0.02	
<i>SAH</i>			
(1) L ⁻ + H ⁺ ⇌ HL	25	10.87 ± 0.03	5.8E - 7
(2) L ⁻ + 2H ⁺ ⇌ H ₂ L ⁺		15.10 ± 0.04	
<i>SAH</i>			
(1) L ⁻ + H ⁺ ⇌ HL	30	10.52 ± 0.03	6.2E - 7
(2) L ⁻ + 2H ⁺ ⇌ H ₂ L ⁺		14.61 ± 0.04	
<i>SAH</i>			
(1) L ⁻ + H ⁺ ⇌ HL	35	10.32 ± 0.04	1.9E - 7
(2) L ⁻ + 2H ⁺ ⇌ H ₂ L ⁺		14.29 ± 0.01	

the rupture of different bonds inside the molecule [56]. From the data obtained we concluded that the molecular weight was in good agreement with this of the calculated molecular weight of the investigated ligand.



Scheme 3. Protonation of SAH hydrazone ligand.

3.6. ^1H NMR spectra

^1H NMR spectra of SAH (Fig. 5) were recorded in $\text{DMSO-}d_6$ solvent. The ^1H NMR spectra of SAH hydrazone ligand showed one singlet at 12.14 ppm corresponding to phenolic $-\text{OH}$ proton and one singlet at 10.31 ppm corresponding to NH proton ($=\text{N}-\text{NH}-$). The signal respect of the proton of ($=\text{N}-\text{CH}$) group of Phthalazine was observed at 8.67 ppm. The signal observed at 8.31 ppm is due to azomethine proton ($-\text{CH}=\text{N}-$) [57,58]. Also, the ^1H NMR spectra of SAH- hydrazone ligand revealed a multiplet at 6.86–7.87 ppm corresponding to aromatic protons [59,60].

3.7. Thermogravimetric analysis

The thermogravimetric (TG) and the derivative thermogravimetric (DTG) plots of Cu^{II} -complex as an illustrative example were given in Fig. 6. The correlations between the different decomposition steps of the complexes with the corresponding weight losses are discussed in terms of the proposed formulae of the complexes. The predicated intermediates and final products were given in Table 4.

The TG and DTG curves of $[\text{Cu}(\text{SAH})\text{Cl}]\cdot\text{H}_2\text{O}$ are shown in Fig. 6. The TGA curve of the $[\text{Cu}(\text{SAH})\text{Cl}]\cdot\text{H}_2\text{O}$ complex shows four stages of decomposition within the temperature range (48–675 °C). The first step of decomposition within the temperature range (48–104 °C) corresponds to the loss of water molecule of hydration with a mass loss 4.6% (calcd. 4.7%). The second step (104–270 °C) corresponds to the loss of half Cl_2 with mass loss 9.5% (calcd. 9.3%). The third step (474–510 °C) corresponds to the loss of $2\text{N}_2 + \text{CH}_4$ molecules with mass loss 18.4% (calcd. 18.9%). The fourth step (510–675 °C) corresponds to the loss of C_{14}H_6 molecule with mass loss 46.6% (calcd. 46.1%). The energies of activation were 42.3, 12.8, 7.8 and 37.6 kJ mol^{-1} for the first, second, third and fourth steps respectively. The total mass loss up to 670 °C is in agreement with the formation of CuO as the final residue (TG 20.84%, calcd. 20.91%).

The TGA curve of the $[\text{Ni}(\text{SAH})\text{Cl}]\cdot\text{H}_2\text{O}$ complex shows three stages of decomposition within the temperature range (48–776 °C). The first step of decomposition within the temperature range (43–180 °C) corresponds to the loss of water molecule of hydration with a mass loss 4.3% (calcd. 4.8%). The second step (259–532 °C) corresponds to the loss of $2\text{N}_2 + 1/2\text{Cl}_2 + \text{CH}_4$ with

mass loss 28.9% (calcd. 28.8%). The third step (532–776 °C) corresponds to the loss of C_{14}H_6 molecule with mass loss 46.6% (calcd. 46.5%). The energies of activation were 17.3, 66.1 and 21.1 kJ mol^{-1} for the first, second and third steps respectively. The total mass loss up to 776 °C is in agreement with the formation of NiO as the final residue (TG 20.2%, calcd. 20.0%).

The TGA curve of the $[\text{Cu}(\text{SAH})\text{Cl}]\cdot\text{H}_2\text{O}$ complex shows four stages of decomposition within the temperature range (41–659 °C). The first step of decomposition within the temperature range (41–120 °C) corresponds to the loss of two water molecules

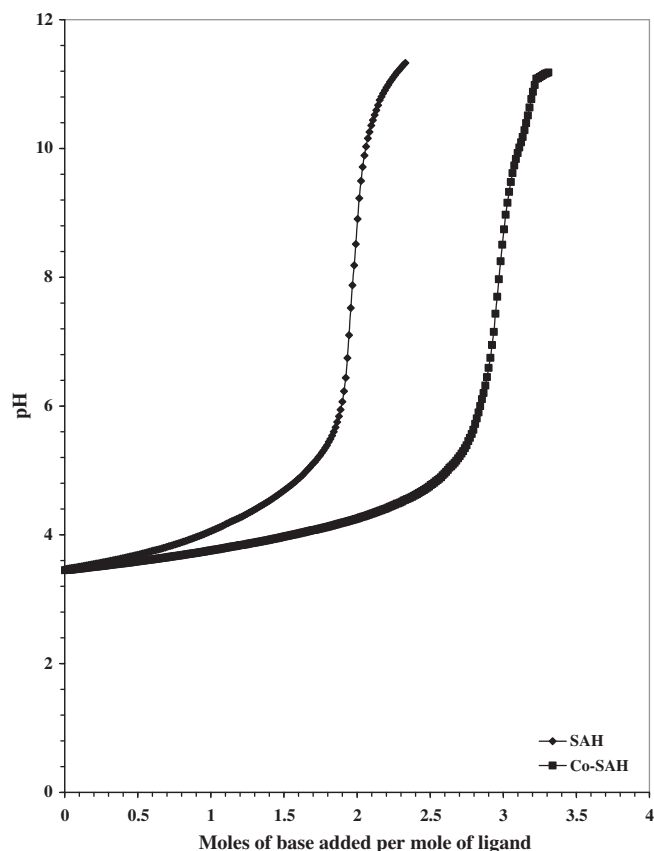


Fig. 8. Potentiometric titration curve for Co-SAH system.

of hydration with a mass loss 9.4% (calcd. 9.1%). The second step (228–367 °C) corresponds to the loss of half Cl₂ with mass loss 9.1% (calcd. 9.0%). The third step (367–402 °C) corresponds to the loss of N₂ molecule with mass loss 7.2% (calcd. 7.1%). The fourth step (402–659 °C) corresponds to the loss of Phthalazine + C₇H₅ molecules with mass loss 56.0% (calcd. 55.6%). The energies of activation were 28.4, 16.2, 16.1 and 44.5 kJ mol⁻¹ for the first, second and third steps respectively. The total mass loss up to 659 °C is in agreement with the formation of CoO as the final residue (TG 18.1%, calcd. 19.1%).

The thermodynamic activation parameters of decomposition processes of complexes namely activation energy (*E_a*), enthalpy (ΔH^*), entropy (ΔS^*) and Gibbs free energy change of the decomposition (ΔG^*) were evaluated graphically by employing the Coats–Redfern relation as follows [61]:

$$\log \left\{ -\log \left[\frac{1-\alpha}{T^2} \right] \right\} = \log \left[\frac{AR}{\theta E_a} \left(1 - \frac{2RT}{E_a} \right) \right] - \frac{E_a}{2.303RT} \quad (3)$$

where α is the fraction of sample decomposed at time *t*, *T* is the derivative peak temperature, *A* the frequency factor, *E_a* the activation energy, *R* the gas constant θ is the heating rate and $(1 - (2RT/E_a)) \cong 1$. A plot of $\log\{-\log(1 - \alpha)/T^2\}$ versus $1/T$ gives a slope from which the *E_a* was calculated and *A* (Arrhenius factor) was determined from the intercept. The entropy of activation was calculated [62]. Fig. 5 represents the linear plots of the thermal decomposition steps of Cu(II)-complex as a representative example of the synthesized complexes. The free energy of activation ΔG^* and the enthalpy of activation ΔH^* were calculated [62]. The kinetic data obtained from the non-isothermal decomposition of the complexes using the appropriate calculation method are cited in Table 5. The negative values of ΔS^* indicate that the reaction rates are slower than normal which is consistent with the results reported previously [63,64] and the positive values of ΔG^* reflected the non-spontaneous nature of process. The correlation coefficients of the thermal decomposition plots were found to lie in the range 0.97–0.99, showing a good fit with linear function. The linear plot of [Cu(SAH)Cl]·H₂O complex as a representation example of M^{II}-SAH complexes was given in Fig. 7. It is clear that the thermal decomposition process of all SAH complexes is non-spontaneous, i.e., the complexes are thermally stable.

3.8. Solution equilibrium studies

3.8.1. Protonation constants of hydrazone ligand (SAH)

Equilibrium studies of SAH hydrazone ligand and its complex formation can not be carried out in aqueous solution because of the nature of the compound involved. These metal complexes as well as SAH hydrazone ligand are insoluble in water. This solvent has been widely used for potentiometric determination of stability constants. The mixture DMSO-water was the chosen solvent for our study. In such a medium, the studied hydrazone ligand and its metal complexes are soluble giving stable solutions. The use of this mixed solvent has some advantages over pure DMSO. Thus, pure DMSO is very hygroscopic and controlling its water content is difficult [65]. This fact would affect reproducibility of our experiment. However, DMSO-water 70:30% mixture has only small hygroscopic character. A further advantage is its compatibility with the standard glass electrode, so that the pH measurements may be carried out in a similar way to that employed in a purely aqueous solution. In contrast, the use of pure DMSO is not recommended for potentiometry. Another advantage of the DMSO-water mixture is its large acidity range ($pK_w = 15.75$) which allows the investigation of deprotonation equilibria of weak acids which could be hardly studied in water [66,67]. The stoichiometric protonation constants of the investigated hydrazone ligand were determined in 70%

DMSO-water mixture at 25 °C and these constants are tabulated in Table 6. Upon addition of NaOH deprotonation of SAH ligand occurs, representation of the acid dissociation constants (*K_a*) in stability study expressed in terms of proton-ligand formation constant or protonation constant Eq. (7), and also used in the present investigation. Analysis of the potentiometric titration curve of SAH- hydrazone ligand using the program Miniquad-75 gave best fit for two protonation constants as proposed by the Eq. (7) (charges are omitted for clarity).

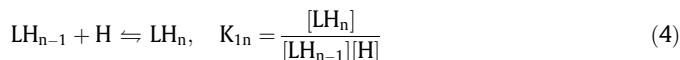


Table 7

Formation constants for binary complexes of (SAH) with metal(II) ions at different temperatures at 70% DMSO-3% H₂O mixture.

System	Temp. (°C)	logβ ^a	S ^b
Cu-SAH	20		
(1) Cu ²⁺ + L ⁻ ⇌ CuL ⁺		12.45 ± 0.02	1.1E - 7
(2) Cu ²⁺ + 2L ⁻ ⇌ CuL ₂		22.65 ± 0.04	
Ni-SAH			
(1) Ni ²⁺ + L ⁻ ⇌ NiL ⁺		11.50 ± 0.03	2.3E - 7
(2) Ni ²⁺ + 2L ⁻ ⇌ NiL ₂		20.18 ± 0.01	
Co-SAH			
(1) Co ²⁺ + L ⁻ ⇌ CoL ⁺		10.98 ± 0.04	3.8E - 7
(2) Co ²⁺ + 2L ⁻ ⇌ CoL ₂		18.95 ± 0.05	
Mn-SAH			
(1) Mn ²⁺ + L ⁻ ⇌ MnL ⁺		9.20 ± 0.02	8.1E - 7
(2) Mn ²⁺ + 2L ⁻ ⇌ MnL ₂		15.90 ± 0.04	
Cu-SAH	25		
(1) Cu ²⁺ + L ⁻ ⇌ CuL ⁺		11.96 ± 0.01	4.0E - 7
(2) Cu ²⁺ + 2L ⁻ ⇌ CuL ₂		21.87 ± 0.02	
Ni-SAH			
(1) Ni ²⁺ + L ⁻ ⇌ NiL ⁺		11.08 ± 0.01	4.5E - 7
(2) Ni ²⁺ + 2L ⁻ ⇌ NiL ₂		19.58 ± 0.08	
Co-SAH			
(1) Co ²⁺ + L ⁻ ⇌ CoL ⁺		10.75 ± 0.02	9.3E - 7
(2) Co ²⁺ + 2L ⁻ ⇌ CoL ₂		18.21 ± 0.02	
Mn-SAH			
(1) Mn ²⁺ + L ⁻ ⇌ MnL ⁺		8.20 ± 0.1	3.9E - 6
(2) Mn ²⁺ + 2L ⁻ ⇌ MnL ₂		14.26 ± 0.1	
Cu-SAH	30		
(1) Cu ²⁺ + L ⁻ ⇌ CuL ⁺		11.35 ± 0.01	4.8E - 7
(2) Cu ²⁺ + 2L ⁻ ⇌ CuL ₂		20.71 ± 0.02	
Ni-SAH			
(1) Ni ²⁺ + L ⁻ ⇌ NiL ⁺		10.75 ± 0.01	3.3E - 7
(2) Ni ²⁺ + 2L ⁻ ⇌ NiL ₂		19.01 ± 0.06	
Co-SAH			
(1) Co ²⁺ + L ⁻ ⇌ CoL ⁺		10.45 ± 0.01	7.6E - 7
(2) Co ²⁺ + 2L ⁻ ⇌ CoL ₂		17.66 ± 0.02	
Mn-SAH			
(1) Mn ²⁺ + L ⁻ ⇌ MnL ⁺		6.89 ± 0.06	5.2E - 7
(2) Mn ²⁺ + 2L ⁻ ⇌ MnL ₂		12.18 ± 0.07	
Cu-SAH	35		
(1) Cu ²⁺ + L ⁻ ⇌ CuL ⁺		10.85 ± 0.05	6.3E - 7
(2) Cu ²⁺ + 2L ⁻ ⇌ CuL ₂		19.66 ± 0.07	
Ni-SAH			
(1) Ni ²⁺ + L ⁻ ⇌ NiL ⁺		10.30 ± 0.03	1.7E - 7
(2) Ni ²⁺ + 2L ⁻ ⇌ NiL ₂		18.39 ± 0.02	
Co-SAH			
(1) Co ²⁺ + L ⁻ ⇌ CoL ⁺		10.10 ± 0.04	8.2E - 7
(2) Co ²⁺ + 2L ⁻ ⇌ CoL ₂		17.09 ± 0.04	
Mn-SAH			
(1) Mn ²⁺ + L ⁻ ⇌ MnL ⁺		6.02 ± 0.07	5.3E - 7
(2) Mn ²⁺ + 2L ⁻ ⇌ MnL ₂		11.02 ± 0.08	

^a Standard deviation is given in parenthesis.

^b Sum of square of residuals.

The two protonation constants are related to the protonation of phenolate, and phthalazine nitrogen atoms, respectively as shown in Scheme 3. Titration with a base produces, in a first stage deprotonation of the protonated phthalazine proton is deprotonated with pK_{a1} value of 4.35 ($pK_{a1} = \log \beta_{012} - \log \beta_{011}$). By further increase of pH, the phenolic proton is deprotonated with pK_{a2} value of 11.11 ($pK_{a2} = \log \beta_{011}$).

3.8.2. Metal^{II} complex formation equilibria

Potentiometric titrations of SAH with Cu^{2+} , Ni^{2+} , Co^{2+} and Mn^{2+} ions were carried out in 1:1 and 1:2 metal–ligand molar ratios at $\mu = 0.1$ M $NaNO_3$ and 25 °C in DMSO–water 70:30% mixture. The deviation in the metal–ligand titration curves from the ligand titration curve implies the formation of metal complexes. The potentiometric titration curve of Co(II)–SAH as a representative example of metal(II)–complexes was given in Fig. 8. The overall formation constants ($\log \beta$) of the species were calculated using Miniquad-75 program. The derived protonation constants of SAH and stepwise formation constants ($\log K$) of complexes are summarized in Tables 6 and 7.

3.9. Correlation of the properties of metal ions with the formation constants of mixed ligand complexes

In an attempt to explain why a given ligand prefers binding to one metal rather than another, it is necessary to correlate the stability constants with the characteristic properties of the metal ions, such as the ionic radius, ionization energy, electronegativity and the atomic number were investigated. Here we have discussed relationships between the properties of central metal ions reported in literature [60,68] and the stability constants of complexes.

The formation constants of M^{II} -complexes of bivalent 3d transition metal ions with SAH are in the order: $Cu^{2+} > Ni^{2+} > Co^{2+} > Mn^{2+}$ in accordance with Irving and Williams order [69]. The correlation between the $\log K_{ML}$ and the reciprocal ionic radii ($1/r$) of the studied bivalent transition metal ions was found to be almost linear. Also, a good linear correlation has been obtained between $\log K_{ML}$ and the electronegativities of the metal ions under study. This in accordance with the fact that increasing electronegativity of the metal ions

($Mn^{2+}(1.55) < Co^{2+}(1.88) < Ni^{2+}(1.91) < Cu^{2+}(2.0)$) will decrease the electronegativity difference between the metal atom and the donor atom of the ligand. Thus, the metal–ligand bond would have more covalent character, which may lead to greater stability of the metal chelates. A good linear relationship has been obtained between $\log K_{ML}$ and the second ionization potential of the bivalent metal ions under study. In general, it is noted that the stability constant of the Cu^{2+} complex is quite large compared to the other metals. The ligand field will give Cu^{2+} some extra stabilization due to tetragonal distortion of the octahedral symmetry [70,71]. Thus, $\log K$ value for the Cu^{2+} -complex deviates significantly when $\log K$ values of metal chelates are plotted against properties of the metal ions. The lower stability of Mn(II) chelates may be due to its larger radius (80).

3.10. Effect of temperature

The values obtained for the thermodynamic parameters ΔH° , ΔS° and ΔG° , associated with the protonation of SAH and its complex formation with Cu(II) species were calculated from the temperature dependence of the data in Table 6. ΔH° and ΔS° were obtained by linear least square fit of $\ln K$ versus $1/T$ ($\ln K = -\Delta H^\circ/RT + \Delta S^\circ/R$) leading to an intercept $\Delta S^\circ/R$ and a slope $-\Delta H^\circ/R$, where K is the equilibrium constant, Figs. 9 and 10. The main conclusions from the data can be summarized as follows.

(I) The protonation reactions of the SAH are exothermic and of comparable ΔH° and ΔS° with a net negative ΔG° . Three factors affect the protonation reactions in Table 6:

- (i) The neutralization reaction, which is an exothermic reaction process.
- (ii) Desolvation of ions, which is an endothermic process.
- (iii) The change of the configuration and the arrangements of the hydrogen bonds around the free and the protonated ligands.

The negative ΔS° indicates that the total number of solvent molecules bound with the dissociated ligand is greater than that originally accompanying the undissociated form.

The stability constants of the complexes formed at different temperatures were calculated and the average values are included in Table 7. From these results the following conclusions can be

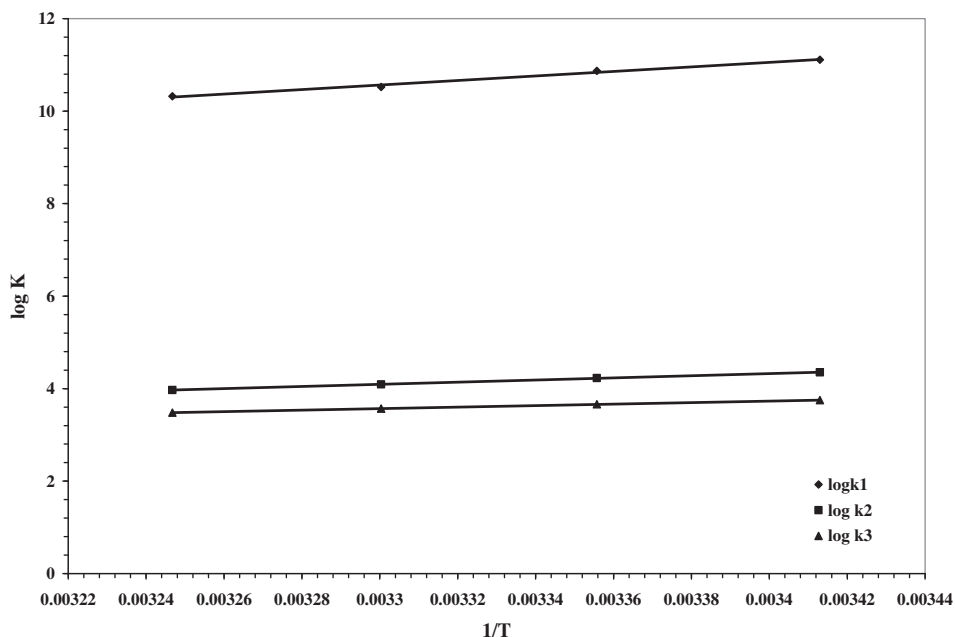


Fig. 9. Effect of temperature on stepwise protonation constant of SAH.

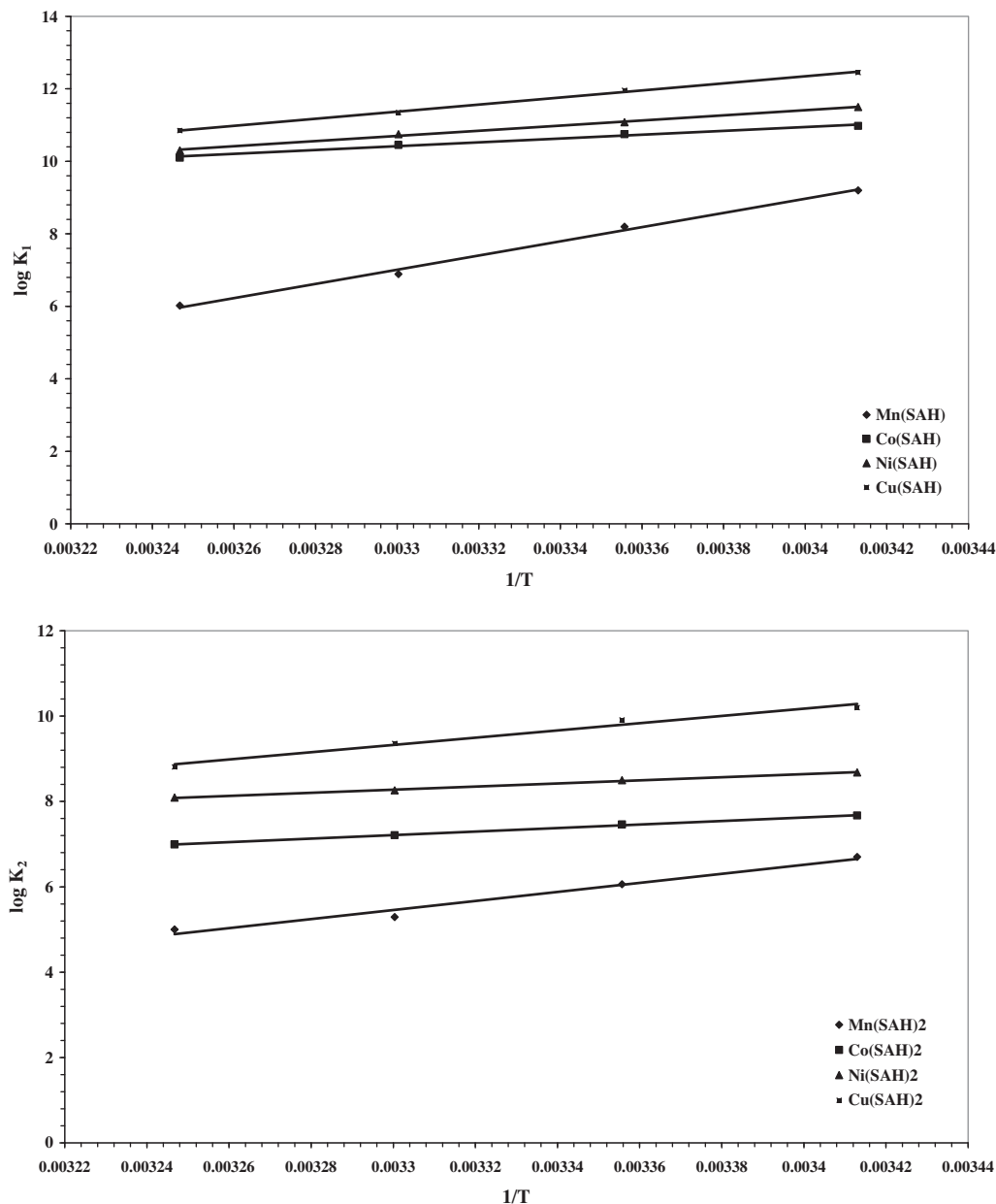


Fig. 10. Effect of temperature on $\ln K$ of $M(II)$ -complexes with SAH-Schiff base.

reached. These values decrease with increasing temperature, confirming that the complexation process is more favorable at lower temperatures. It is known that the divalent metal ions exist in solution as octahedrally hydrated species [72] and the obtained values of ΔH and ΔS can then be considered as sum of two contributions: (a) release of H_2O molecules and (b) metal–ligand bond formation. From these results the following conclusions can be made.

1. Table 7 shows that $(\log K_1 - \log K_2)$ values are usually positive, since the coordination sites of the metal ions are more freely available for binding of the first molecule than the second one.
2. For the same ligand at constant temperature, the stability of the chelates increases in the order $Cu^{2+} > Ni^{2+} > Co^{2+} > Mn^{2+}$ [69]. This order largely reflect the changes in the heat of complex formation across the series from a combination of the influence of both the crystal field stabilization energies [72] and the polarizability of the metal ion [73].

3. All values of ΔG° for complexation are negative (Table 8), indicating that the chelation process proceeds spontaneously.
4. The negative values of ΔH° show that the chelation process is exothermic, indicating that the complexation reactions are favored at low temperatures.
5. The entropy term (ΔS°) for the complexation reactions is negative, which is in consistency with the protonation reaction of the ligand. The negative entropy changes together with the high negative enthalpy change contribute to the favorable free energy change of the complex formation reactions.

3.11. Species distribution curves of metal(II)-SAH complexes

Estimation of equilibrium concentrations of metal(II) complexes as a function of pH provides a useful picture of metal ion binding in solutions. All of the species distributions were calcu-

lated with the aid of the Species computer program [31]. The concentrations of metal ligand complexes increase with increasing of pH. The species distribution pattern for Cu-(SAH), taken as a representative of metal ligand complexes, is given in Fig. 11. Cu(SAH) complex starts to form at pH ~ 2.6 and reaches its maximum concentration 84% at pH ~ 3.8. Also, Cu(SAH)₂ complex starts to form at pH ~ 3.6 and reaches its maximum concentration 97% at pH ~ 7.4.

3.12. Biological activity

The biological activity of the metal complexes is governed by the following factors: (i) the chelate effect of the ligands, (ii) the nature of the donor atoms, (iii) the total charge on the complex ion, (iv) the nature of the metal ion, (v) the nature of the counter ions that neutralize the complex, and (vi) the geometrical structure of the complex [74]. Furthermore, chelation reduces the polarity of the metal ion because of partial sharing of its positive charge with the donor groups and possibly the π -electron delocalization within the whole chelate ring system that is formed during coordination [75]. These factors increase the lipophilic nature of the central metal atom and hence increasing the hydrophobic character and liposolubility of the molecule favoring its permeation through the lipid layer of the bacterial membrane. This enhances the rate of uptake/entrance and thus the antibacterial activity of the testing compounds. The hydrazone SAH ligand and its chelates (1–3) were tested for their inhibitory effects on the growth of two Gram positive (*S. aureus*, *Bacillus subtilis*) and two Gram negative (*E. coli*, *Pseudomonas aeruginosa*) bacteria at concentration of 20 mg/ml in DMSO as solvent using Ampicillin as standard material and fungi: *A. flavus* and *C. albicans* using Amphotericin as standard material because such organisms can achieve resistance to antibiotics through biochemical and morphological modification [76]. The antibacterial and antifungal activities of the new compounds are listed in Tables 9 and 10 and represented graphically in Fig. 12. The antibacterial activity was tested by using the disc diffusion method. The antimicrobial results showed that:

- (1) The hydrazone SAH ligand is biologically active and its activity may be arise from the hydroxyl groups which may play an important role in the antibacterial activity [77], as well as the presence of imine group which imports in elucidating the mechanism of transformation reaction in biological systems [78].

Table 8
Thermodynamic parameters for the protonation equilibria of SAH and formation equilibria of metal(II)-SAH complexes.

Equilibrium	ΔH kJ mol ⁻¹	ΔS JK ⁻¹ mol ⁻¹	ΔG kJ mol ⁻¹
SAH			
(1) $L^- + H^+ \rightleftharpoons HL$	-94.03	-108	-61.83
(2) $HL + H^+ \rightleftharpoons H_2L^+$	-44.23	-67.58	-24.09
Cu-SAH			
(2) $Cu^{2+} + L^- \rightleftharpoons CuL^+$	-186.9	-399	-68.01
(3) $CuL^+ + L^- \rightleftharpoons CuL_2$	-162.7	-358.6	-55.92
Ni-SAH			
(2) $Ni^{2+} + L^- \rightleftharpoons NiL^+$	-135.8	-242.6	-63.47
(3) $NiL^+ + L^- \rightleftharpoons NiL_2$	-69.46	-70.69	-48.41
Co-SAH			
(2) $Co^{2+} + L^- \rightleftharpoons CoL^+$	-101.5	-135.2	-61.16
(3) $CoL^+ + L^- \rightleftharpoons CoL_2$	-79.11	-122.9	-42.48
Mn-SAH			
(2) $Mn^{2+} + L^- \rightleftharpoons MnL^+$	-375	-1103	-46.26
(3) $MnL^+ + L^- \rightleftharpoons MnL_2$	-375	-566.2	-34.51

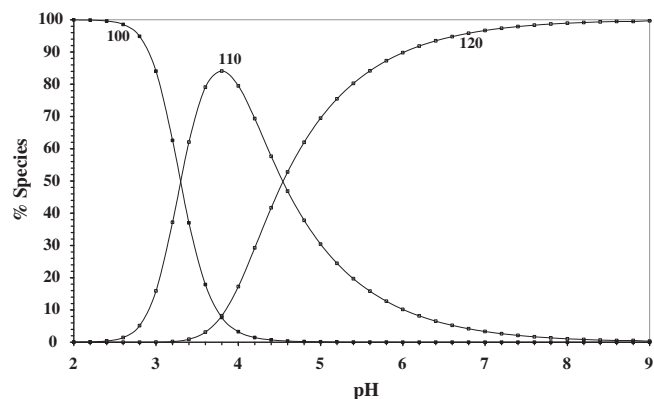


Fig. 11. Concentration distribution of various species as a function of pH in the Cu-SAH system.

- (2) The synthesized compounds were found to be more toxic compared with their parent hydrazone ligand against the same micro-organism and under the identical experimental conditions. The increase in biological activity of the metal chelates may be due to the effect of the metal ion on the normal cell process. A possible mode of toxicity increase may be considered in the light of Tweedy's chelation theory [79]. Chelation considerably reduce the polarity of the metal ion because of partial sharing of its positive charge with the donor group and possible π -electron delocalization within the whole chelate ring system that is formed during coordination. Such chelation could enhance the lipophilic character of the central metal atom and hence increasing the hydrophobic character and liposolubility of the complex favoring its permeation through the lipid layers of the cell membrane. This enhances the rate of uptake/entrance and thus the antimicrobial activity of the testing compounds. Accordingly, the antimicrobial activity of the isolated complexes can be referred to the increase of their lipophilic char-

Table 9
Antibacterial activity of M(II)-SAH complexes.

Compounds	Parameters	Diameter of inhibition zone (in mm) (G ⁻)			
		<i>P. aeruginosa</i>	<i>E. coli</i>	<i>B. subtilis</i>	<i>S. aureus</i>
Conc. (mg/ml)		20.0	20.0	20.0	20.0
SAH	$\log K_1^H$ 10.87	11	11	12	12
	$\log K_2^H$ 4.23				
Cu ^{II}	$\log K$ 11.96	15	14	15	14
Ni ^{II}	$\log K$ 11.08	13	13	12	13
Co ^{II}	$\log K$ 10.75	0	12	0	0
Ampicillin	-	17	22	20	18
DMSO (control)	-	0	0	0	0

Table 10
Antifungal activity of M(II)-SAH complexes.

Compounds	Parameters	Diameter of inhibition zone (in mm)	
		<i>A. flavus</i>	<i>C. albicans</i>
Conc. (mg/ml)		20.0	20.0
SAH	$\log K_1^H$ 10.87	10	10
	$\log K_2^H$ 4.23		
Cu ^{II}	$\log K$ 11.96	13	14
Ni ^{II}	$\log K$ 11.08	11	12
Co ^{II}	$\log K$ 10.75	10	11
Amphotericin (B)	-	17	17
DMSO (control)	-	0	0

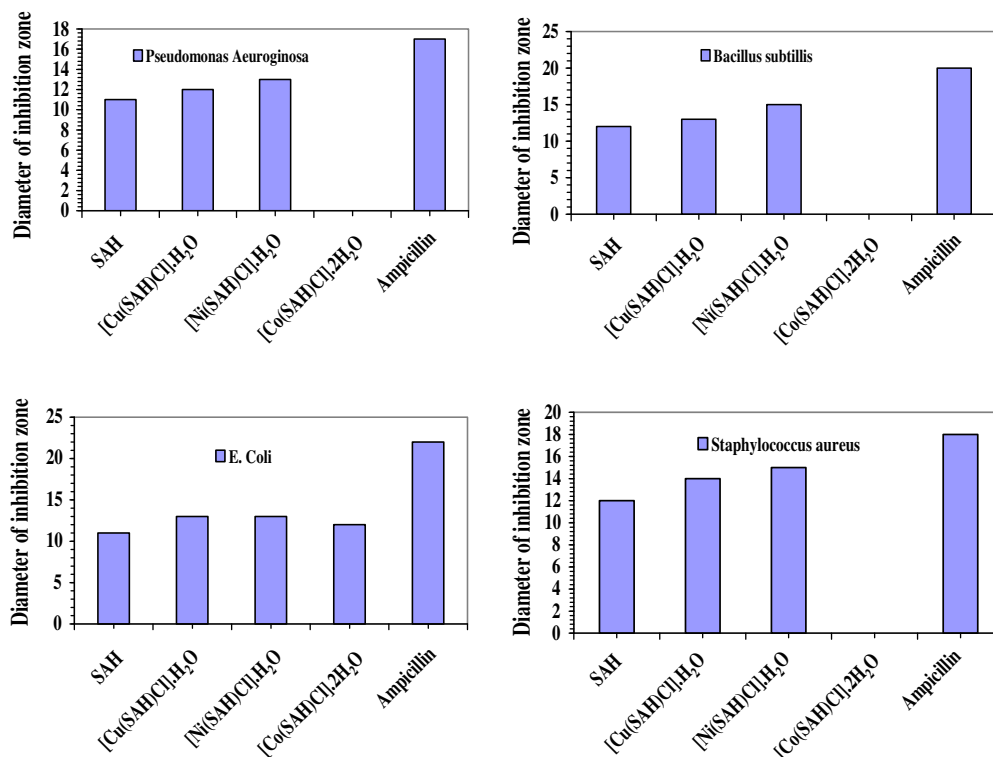


Fig. 12. Biological activity of metal complexes towards different types of bacterial strains.

- acter which in turn deactivates enzymes responsible for respiration processes and probably other cellular enzymes, which play a vital role in various metabolic pathways of the tested micro-organisms. Furthermore, the mode of action of the compounds may involve the formation of a hydrogen bond through the azomethine nitrogen atom (>C=N) with the active centers of cell constituents, resulting in interference with the normal cell process [80].
- (3) From the above mentioned points, structure activity relationships evidence that the complexation with copper enhances the antimicrobial activity of the ligands against some of the tested organisms. Since copper chelates have an enhanced antimicrobial activity, in comparison to their analogous containing metal(II) and nickel(II) ions, the metal seems to play a relevant role in the activity of these compounds. A similar behavior of the increased antibacterial activity was also exhibited by copper derivatives of 2,6-diacetylpyridine bis (2-thenoylhydrazone) in comparison to the corresponding Co(II) and Ni(II) chelates [81,82].
- (4) The tested complexes were more active against Gram-positive than Gram-negative bacteria, it may be concluded that the antimicrobial activity of the compounds is related to cell wall structure of the bacteria. It is possible because the cell wall is essential to the survival of bacteria and some antibiotics are able to kill bacteria by inhibiting a step in the synthesis of peptidoglycan. Gram-positive bacteria possess a thick cell wall containing many layers of peptidoglycan and teichoic acids, but in contrast, Gram negative bacteria have a relatively thin cell wall consisting of a few layers of peptidoglycan surrounded by a second lipid membrane containing lipopolysaccharides and lipoproteins. These differences in cell wall structure can produce differences in antibacterial susceptibility and some antibiotics can kill only Gram-positive bacteria and is ineffective against Gram-negative pathogens [83].

- (5) The antibacterial activity can be ordered as [Cu(SAH)] > [Ni(SAH)] > [Co(SAH)], suggesting that the lipophilic behaviour increases in the same order. This in accordance also with the stability constants order $\log K_{\text{Cu-SAH}} = 11.96 > \log K_{\text{Ni-SAH}} = 11.08 > \log K_{\text{Co-SAH}} = 10.75$.
- (6) The results indicate that, the three complexes exhibited moderate activity against the fungal strains when compared with standard *Amphotericin*.
- (7) The variation in the effectiveness of different compounds against different organisms depends on either the impermeability of the cells of the microbes or on differences in ribosome of microbial cells [74].
- (8) The importance of such work lies in the possibility that the new compounds might be more effective drugs against bacteria for which a thorough investigation regarding the structure-activity relationship, toxicity and in their biological effects which could be helpful in designing more potent antibacterial agents for therapeutic use.

Conclusions

A series of three coordinated transition metal(II) complexes have been synthesized by the reaction of metal chloride with the tridentate NNO hydrazone (SAH), which was prepared by the condensation of salicylaldehyde with hydralazine. The synthetic procedure in this work resulted in the formation of complexes in the molar ratio (1:1) (Cu:SAH). The newly synthesized hydrazone participated in bonding to copper as monobasic tridentate ligand through the azomethine-N, phthalazine-N and phenolic oxygen atom via deprotonation forming stable six and five membered rings. The ionization constants of the investigated ligands have been determined potentiometrically. The complex formation equilibria were investigated to ascertain the composition and stability constants of the complexes. The concentration distribu-

tion diagrams of the complexes were evaluated. The antibacterial activity results indicated that tested complexes were more active against Gram-positive than Gram-negative bacteria. It may be concluded that antibacterial activity of the compounds is related to cell wall structure of the bacteria. It is possible because the cell wall is essential to the survival of many bacteria and some antibiotics are able to kill bacteria by inhibiting a step in the synthesis of peptidoglycan. The antibacterial activity of the isolated metal chelates obeyed this order $[Cu(SAH)] > [Ni(SAH)] > [Co(SAH)]$ which is in accordance with the stability constants order $\log K_{Cu-SAH} = 11.96 > \log K_{Ni-SAH} = 11.08 > \log K_{Co-SAH} = 10.75$.

References

- [1] J.J.R.F.D. Silva, R.J.P. Williams, *The Biological Chemistry of the Elements*, Clarendon Press, Oxford, 1991.
- [2] C. Sousa, C. Freire, B. de Castro, *Molecules* 8 (2003) 894.
- [3] V.K. Singh, R. Sinha, R. Kant, B.K. Sinha, *Asian J. Chem.* 10 (1998) 532.
- [4] L.T. Yildirim, O. Atakol, *Cryst. Res. Technol.* 37 (2002) 1352.
- [5] A. Pui, *Croat. Chem. Acta* 75 (2002) 165.
- [6] A.D. Garvnovski, A.L. Nivorozhkin, V.I. Minkin, *Coord. Chem. Rev.* 126 (1993) 1.
- [7] M.J.M. Campbell, *Coord. Chem. Rev.* 15 (1975) 279.
- [8] D.R. Williams, *Chem. Rev.* 72 (1972) 203.
- [9] A. Furst, R.T. Haro, *Prog. Exp. Tumor Res.* 12 (1969) 102.
- [10] F.B. Dwyer, E. Mayhew, E.M.F. Roe, A. Shulman, *Br. J. Cancer* 19 (1965) 195.
- [11] X.M. Ouyang, B.L. Fei, T.A. Okamuro, W.Y. Sun, W.X. Tang, N. Ueyama, *Chem. Lett.* 362 (2002).
- [12] N. Raman, Y.P. Raja, A. Kulandaisamy, *Proc. Indian Acad. Sci. (Chem. Sci.)* 113 (2001) 183.
- [13] C. Jayabalakrishnan, K. Natarajan, *Trans. Met. Chem.* 27 (2002) 75.
- [14] M.M.A. Mohamed, A.A. El-Sherif, *J. Solution Chem.* 39 (2010) 639.
- [15] A.A. El-Sherif, M.M. Shoukry, *J. Coord. Chem.* 58 (16) (2005) 1401.
- [16] A.A. El-Sherif, M.M. Shoukry, *Spectrochim. Acta Part A* 66 (2007) 691.
- [17] A.A. El-Sherif, M.M. Shoukry, *Inorg. Chim. Acta* 360 (2007) 473.
- [18] A.A. El-Sherif, *J. Solution Chem.* 39 (2010) 1562.
- [19] A.A. El-Sherif, *Inorg. Chim. Acta* 362 (2009) 4991.
- [20] F.J. Welcher, *The Analytical Uses of Ethylenediamine Tetraacetic Acid*, Van Nostrand, Princeton, 1965.
- [21] A.W. Bauer, W.M. Kirby, C. Sherris, M. Turck, Antibiotic susceptibility testing by a standardized single disk method, *J. Am. Clin. Pathol.* 45 (1966) 493.
- [22] M.A. Pfaller, L. Burmeister, M.A. Bartlett, M.G. Rinaldi, *J. Clin. Microbiol.* 26 (1988) 1437.
- [23] National Committee for Clinical Laboratory Standards (1993), Methods for dilution antimicrobial susceptibility tests for bacteria that grow aerobically. Approved standard M7–A3, Villanova, Pa.
- [24] National Committee for Clinical Laboratory Standards (2002), reference method for broth dilution antifungal susceptibility testing of conidium-forming filamentous fungi: proposed standard M38–A, NCCLS, Wayne, PA, USA.
- [25] National Committee for Clinical Laboratory Standards (2003), method for antifungal disk diffusion susceptibility testing of yeast: proposed guideline M44–P, NCCLS, Wayne, PA, USA.
- [26] L.D. Liebowitz, H.R. Ashbee, E.G.V. Evans, Y. Chong, N. Mallatova, M. Zaidi, D. Gibbs, *Microbiol. Infect. Dis.* 24 (2001) 27.
- [27] M.J. Matar, L. Ostrosky-Zeichner, V.L. Paetznick, J.R. Rodriguez, E. Chen, J.H. Rex, *Antimicrob. Agents Chemother.* 47 (2003) 1647.
- [28] T. Gündüz, E. Kılıç, F. Köseoğlu, E. Canel, *Anal. Chim. Acta* 282 (1993) 489.
- [29] E.P. Serjant, *Potentiometry and Potentiometric Titrations*, Wiley, New York, 1984.
- [30] P. Gans, A. Sabatini, A. Vacca, An improved computer program for the computation of formation constants from potentiometric data, *Inorg. Chim. Acta* 18 (1976) 237.
- [31] L. Pettit, Univ. Leeds, Personal Communication.
- [32] W.J. Geary, *Coord. Chem. Rev.* 7 (1971) 81.
- [33] L.K. Thompson, F.L. Lee, E.J. Gabe, *Inorg. Chem.* 27 (1988) 39.
- [34] Z.M. Zaki, S.S. Haggag, A.A. Soayed, *Spectro. Lett.* 31 (4) (1983) 757.
- [35] L.J. Bellamy, *The Infrared Spectra of Complex Molecules*, second ed., J. Wiley, New York, 1964.
- [36] S.K. Sahoo, M. Baral, B.K. Kanungo, *Polyhedron* 25 (2006) 722.
- [37] A. Kulkarni, S.A. Patil, P.S. Badami, *Eur. J. Med. Chem.* 44 (2009) 2904.
- [38] S. Sarkar, K. Dey, *Spectro. Acta Part A* 62 (2005) 383.
- [39] K.K. Narang, V.P. Singh, *Trans. Met. Chem.* 18 (1993) 287.
- [40] D.X. West, A.A. Nassar, *Trans. Met. Chem.* 23 (1998) 321.
- [41] G.B. Bagihalli, P.G. Avaji, S.A. Patil, P.S. Badami, *Eur. J. Med. Chem.* 43 (2008) 2639.
- [42] K.C. Satpathy, A.K. Panda, R. Mishra, A.P. Chapdar, S.K. Pradhan, *J. Indian Chem. Soc.* 71 (1994) 593.
- [43] A.S. El-Tabl, F.A. El-Saied, A.N. Al-Hakimi, *Trans. Met. Chem.* 32 (2007) 689.
- [44] D.X. West, N.M. Kozub, G.A. Bain, *Trans. Met. Chem.* 21 (1996) 52.
- [45] M.A. Ali, S.G. Teoh, *J. Inorg. Nucl. Chem.* 41 (1979) 809.
- [46] R. Atkins, G. Brewer, E. Kokot, G.M. Mockier, E. Sinn, *Inorg. Chem.* 24 (1985) 127.
- [47] V. Ravindar, S.J. Swamy, S.S. Srihari, P. Longaiah, *Polyhedron* 4 (1985) 1511.
- [48] P.S. Reddy, K.H. Reddy, *Polyhedron* 19 (2000) 1687.
- [49] M.F. Iskander, T.E. Khalil, R. Werner, W. Hasse, I. Svoboda, H. Fuess, *Polyhedron* 19 (2000) 1181.
- [50] N. Singh, *BioMetals* 16 (2003) 311.
- [51] R. Dingle, *Inorg. Chem.* 10 (1971) 1141.
- [52] K. Singh, M.S. Barwa, P. Tyagi, *Eur. J. Med. Chem.* 42 (3) (2007) 394.
- [53] J. Morales-Juárez, J. Pastor-Medrano, R. Cea-Olivares, V. García-Montalvo, R.A. Toscano, *Polyhedron* 26 (4) (2007) 918.
- [54] R.L. Dutta, A. Syamal, *Elements of Magnetochemistry*, second ed., Affiliated East–West Press Pvt. Ltd., New Delhi, 1993.
- [55] A.B.P. Lever, *Inorganic Electronic Spectroscopy*, Second ed., Elsevier, Amsterdam, 1984.
- [56] *British Pharmacopia*, Her Majesty's Stationery Office, London, UK, 1998, p. 1040.
- [57] S. Rao, *Asian J. Chem.* 17 (2005) 2663.
- [58] M. Odabaşoğlu, F. Arslan, H. Olmez, O. Buyukgungor, *Dyes Pigments* 75 (2007) 507.
- [59] H. Nseimi, J. Safari, A. Heidarneshad, *Dyes Pigments* 73 (2007) 251.
- [60] A.A. El-Sherif, T.M.A. Eldebss, *Spectrochim. Acta Part A* 79 (2011) 1803.
- [61] A.W. Coats, J.P. Redfern, *Nature* 201 (1964) 68.
- [62] S. Glasstone, *Textbook of Physical Chemistry*, second ed., Macmillan, Bombay, India, 1974.
- [63] M. Lalia-Kantouri, G.A. Katsoulos, C.C. Hadjikostas, P. Kokorotsikos, *J. Therm. Anal.* 35 (7) (1989) 2411.
- [64] N.A. Al-Awadi, N.M. Shuaib, A. Abbas, A.A. El-Sherif, A. El-Dissouky, E. Al-Saleh, *Bioinorg. Chem.* 2007 (Article ID 79,897).
- [65] H. Koksai, M. Dolaz, M. Tumer, S. Serin, *Synth. React. Inorg. Met.–Org. Chem.* 31 (2001) 1141.
- [66] D. Martin, H.G. Hauthal, *Dimethyl Sulphoxide*, Van Nostrand Reinhold, Workingham, UK, 1975.
- [67] R. Hernandez-Molina, A. Mederos, P. Gili, S. Dominquez, P. Numez, G. Grmain, T. Debaerdemaeker, *Inorg. Chim. Acta* 256 (1997) 319.
- [68] J.E. Huheey, *Inorganic Chemistry*, Harper SI Edn, New York, 1983.
- [69] H. Irving, R.J.P. Williams, *Analyst (London)* 77 (1952) 813.
- [70] M.T. Beck, *Chemistry of Complex Equilibria*, Akademiai Kiado, Budapest, 1970.
- [71] F.A. Cotton, G. Wilkinson, *Inorg. Chem.*, Wiley, London, 1962.
- [72] C.S.G. Phillips, R.J.P. Williams, *Inorg. Chem.*, Oxford, 1966. Vol. 2.
- [73] F.R. Harlly, R.M. Burgess, R.M. Alcock, *Solution Equilibria*, Ellis Harwood, Chichester, 1980. p. 257.
- [74] P.G. Lawrence, P.L. Harold, O.G. Francis, *Antibiot. Chemother.* 5 (1980) 1597.
- [75] E.K. Efthimiadou, G. Psomas, Y. Sanakis, N. Katsaros, A. Karaliota, *J. Inorg. Biochem.* 101 (2007) 525.
- [76] S. Çakir, E. Bicer, M. Odabaşoğlu, Ç. Albayrak, *J. Braz. Chem. Soc.* 4 (2005) 711.
- [77] A.S.A. Zidan, *Phosphorus Sulfur Silicon* 178 (2003) 567.
- [78] N. Sari, S. Arslan, E. Logoglu, I. Sakiyan, *J. Sci.* 16 (2003) 283.
- [79] B.G. Tweedy, *Phytopathology* 55 (1964) 910.
- [80] N. Dharmaraj, P. Viswanathamurthi, K. Natarajan, *Trans. Met. Chem.* 26 (2001) 105.
- [81] S.C. Singh Jadon, N. Gupta, R.V. Singh, *Indian J. Chem.* 34A (1995) 733.
- [82] M. Carcelli, P. Mazza, C. Pelizzi, G. Pelizzi, F. Zani, *J. Inorg. Biochem.* 57 (1995) 43.
- [83] A.L. Koch, *Clin. Microbiol. Rev.* 16 (2003) 673.